An Implicit Transition Matrix Approach to Stability Analysis of Flexible Multi-Body Systems *

Olivier A. Bauchau and Yuri G. Nikishkov
School of Aerospace Engineering,
Georgia Institute of Technology,
Atlanta, Georgia, USA.

Abstract

The stability of linear systems defined by ordinary differential equations with constant or periodic coefficients can be assessed from the spectral radius of their transition matrix. In classical applications of this theory, the transition matrix is explicitly computed first, then its eigenvalues are evaluated; if the largest eigenvalue is larger than unity, the system is unstable. The proposed implicit transition matrix approach extracts the dominant eigenvalues of the transition matrix using the Arnoldi algorithm, *without the explicit computation of this matrix*. As a result, the proposed implicit method yields stability information at a far lower computational cost than that of the classical approach, and is ideally suited for stability computations of systems involving a large number of degrees of freedom. Examples of application of the proposed methodology to flexible multi-body systems are presented that demonstrate its accuracy and computational efficiency.

1 Introduction

An important aspect of the dynamic response of flexible multi-body systems is the potential presence of instabilities. The instability of a cantilevered beam subjected to a tip, compressive follower force [1], or the instabilities appearing in rotor dynamics [2, 3] are but two well-known types instabilities that can occur in dynamical systems and flexible multi-body systems. If the equations of motion of the system can be cast in the form of ordinary differential equations with constant coefficients, classical stability analysis methodologies based on the characteristic exponents of the system can be used. On the other hand, when the equations of motion of the system can be cast in the form of ordinary differential equations with periodic coefficients, Floquet theory [4, 5] is used. Stability analysis is typically performed on simplified models with the smallest number of degrees of freedom required to capture

* *Multibody Systems Dynamics*, **5**, pp 279 – 301, 2001

the physical phenomenon that causes the instability. As the number of degrees of freedom used to represent the system increases, these methods become increasingly cumbersome, and quickly unmanageable.

Due to increased available computer power, the analysis of flexible multi-body systems relies on increasingly complex, large scale models. Full finite element analysis codes are now routinely used for this purpose [6, 7, 8]. These codes should provide increasingly reliable predictions of the dynamic response of multi-body systems and stability can be assessed from the response of such simulations. If the response to an initial perturbation grows in time, the system is unstable, on the other hand, if the response decays, the system is stable. Unfortunately, this approach only provides qualitative results: it is difficult to compute damping rates from the response. Furthermore, this approach is prone to errors: if the system is not simulated for a long enough period, an unstable system could be mistaken for a stable one, or vice versa. Consequently, stability analysis methodologies are needed that can extract stability information and damping rates from large scale simulation tools.

It can be shown [4, 5] that the stability of linear system defined by ordinary differential equations with constant or periodic coefficients can be assessed from the spectral radius their transition matrix. In classical applications of this theory, the transition matrix is explicitly computed first, then its eigenvalues are evaluated; if the largest eigenvalue is larger than unity, the system is unstable. For stable systems, damping rates can be evaluated from the dominant eigenvalues of the transition matrix.

The transition matrix relates all the states of the system at a given instant to the same states at a later time, and its size is equal to the total number of states of the system. Typically, the columns of the transition matrix are computed one at a time, and correspond to the responses of the system after a period of time to linearly independent initial conditions. As a result, the computation of the transition matrix of a system with N states requires N integrations of the system response over a period of time for a set of N linearly independent initial conditions. As the number of degrees of freedom increases, the computational burden associated with the evaluation of the transition matrix becomes overwhelming. Consequently, this approach has been limited to system with relatively few states, say $N \leq 100$, and seems inappropriate for large scale systems.

In this paper, a novel approach is proposed, the implicit transition matrix approach, which evaluates the dominant eigenvalues of the transition matrix using the Arnoldi algorithm, without the explicit computation of this matrix. This method is far more computationally efficient than the classical approach and is ideally suited for systems involving a large number of degrees of freedom. The paper is structured in the following manner. Section 2 presents a framework for stability analysis of linear systems with constant or periodic coefficients. The Arnoldi algorithm is reviewed in section 3, and the proposed implicit transition matrix approach is presented in section 4. Section 5 describes numerical applications that validate the proposed method and demonstrate its accuracy and efficiency.

2 Stability Analysis Based on the Transition Matrix

Consider a set of ordinary differential equations [4] with periodic coefficients governed by the following N first order differential equations

$$\dot{\underline{X}} = A(t)\ \underline{X}, \tag{1}$$

where t denotes time and $\dot{()}$ a derivative with respect to time, $A(t+T) = A(t)$ is a periodic matrix, T the period of the system, and $\underline{X}$ a column vector of system states. Note that when $A(t) = A$ is a constant matrix, this represents a set of ordinary differential equations with constant coefficients, and the period of the system is arbitrary. Let $\Psi(t)$ be a fundamental matrix solution of eq. (1)

$$\dot{\Psi}(t) = A(t)\ \Psi(t). \tag{2}$$

In view of the periodic nature of matrix A, it is clear that

$$\dot{\Psi}(t+T) = A(t+T)\ \Psi(t+T) = A(t)\ \Psi(t+T). \tag{3}$$

This shows that $\Psi(t+T)$ is also a fundamental matrix solution of the same system. Linearity guarantees that two fundamental matrix solutions $\Psi(t+T)$ and $\Psi(t)$ are uniquely dependent.

The transition matrix $\Phi(t,T)$ relates the states of the system at time t and $t+T$,

$$\underline{X}(t+T) = \Phi(t,T)\ \underline{X}(t). \tag{4}$$

It then follows from definition of fundamental matrix solution that

$$\Psi(t+T) = \Phi(t,T)\ \Psi(t). \tag{5}$$

Suppose that all eigenvalues of the transition matrix are distinct; the following eigen-decomposition [9] then exists

$$P^{-1}\ \Phi(t,T)\ P = D = \mathrm{diag}(\Lambda_1, \ldots, \Lambda_N), \tag{6}$$

where P is a nonsingular matrix, D is a diagonal matrix of eigenvalues, all dependent on initial time t. Pre-multiplying eq. (5) by the inverse of P and recursively yields

$$\Gamma(t+nT) = D^n\ \Gamma(t), \tag{7}$$

where $P\ \Gamma(t) = \Psi(t)$, n is an integer. As $n \to \infty$, this relationship yields the behavior of the fundamental matrix solution as $t \to \infty$. The solution is stable if $|\Lambda_p| \leq 1$ for all $1 \leq p \leq N$. In other words, *the system defined by eqs. (1) is stable if and only if the spectral radius of the transition matrix is less or equal to unity, i.e.*

$$\rho(\Phi(t,T)) \leq 1. \tag{8}$$

Note that this result is identical to that obtained from the general Floquet theory [4, 5] for linear systems with periodic coefficients.

If the system has constant coefficients, the solution of eqs. (1) is [4]

$$\underline{X}(t) = e^{tA}\ \underline{X}_0. \tag{9}$$

In view of eq. (4), $\Phi(0,T) = e^{TA}$. If λ_p are the eigenvalues of A, it can be readily shown that the eigenvalues of e^{TA} are $e^{T\lambda_p}$, and it follows that $\Lambda_p = e^{T\lambda_p}$. Hence, the eigenvalues λ_p and Λ_p of the system matrix A and transition matrix $\Phi(0,T)$, respectively, are related by

$$\lambda_p = \frac{1}{T} \ \ln \ \Lambda_p = \zeta_p + j\omega_p = \frac{1}{T} \ \ln \ |\Lambda_p| + j \ \frac{1}{T} \ \arctan \frac{\Im(\Lambda_p)}{\Re(\Lambda_p)}, \tag{10}$$

where $j = \sqrt{-1}$. Hence, the system damping rates ζ_p and frequencies ω_p can be computed from the eigenvalues of the transition matrix.

The above developments provide a framework for stability analysis of linear systems with constant or periodic coefficients. The procedure is conveniently broken into the following three steps

1. *Evaluate the transition matrix.* Eq. (4) suggests the following method: select N independent initial conditions $Y(0) = I$ and integrate the governing equation (1) for each set of initial conditions to find $\Phi(0,T) = Y(T)$.

2. *Evaluate the eigenvalues of the transition matrix.* This requires the solution of a standard eigenproblem, which can be readily obtained with the help of linear algebra software packages.

3. *Use stability criterion (8)* to assess system stability.

This approach has been widely used for the assessment of stability of systems with periodic coefficients [10]. Among many other researchers, Hsu [11, 12] applied this methodology to general linear systems with periodic coefficients, and Peters [13] and Friedmann [14] to rotorcraft stability analysis.

The above discussion clearly shows the difficulties associated with the application of transition matrix approach to stability assessment. The evaluation of the transition matrix can become an overwhelming task as it requires one integration of the system of equations over a period of time for each state of the system. As the number of states increases this computational effort becomes prohibitive.

3 The Arnoldi Algorithm

One of the most reliable methods of extracting the eigenvalues of a general, unsymmetric matrix Φ of size $N \times N$ is the Arnoldi algorithm [15, 9]. This algorithm is based on the iterative construction of a Krylov subspace

$$\mathcal{K}_j(\Phi, \underline{b}) = \left[\underline{b}, \Phi\underline{b}, \Phi^2\underline{b}, \ldots, \Phi^{j-1}\underline{b}\right], \tag{11}$$

where $\underline{b}$ is an arbitrary vector. The basis idea is to use this subspace to reduce Φ to an upper Hessenberg matrix H.

A new vector $\underline{q}_{j+1}$ of the Krylov subspace will be constructed using the following recurrence formula

$$h_{j+1,j} \ \underline{q}_{j+1} = \Phi \ \underline{q}_j - \sum_{i=1}^{j} h_{i,j} \ \underline{q}_j = \underline{r}_j. \tag{12}$$

It is desirable to normalize $\underline{q}_{j+1}$, *i.e.* $|\underline{q}_{j+1}| = 1$, implying

$$h_{j+1,j} = ||\underline{r}_j||. \tag{13}$$

Furthermore, $\underline{q}_{j+1}$ is made orthogonal to all previous vectors $\underline{q}_j$, such that

$$h_{i,j} = \underline{q}_i^T \ \Phi \ \underline{q}_j. \tag{14}$$

The basic recurrence relationship, eq. (12), is conveniently written in a matrix form as

$$\Phi \ \underline{q}_j = \lfloor \underline{q}_1, \underline{q}_2, \ldots, \underline{q}_j \rfloor \begin{bmatrix} h_{1,j} \\ h_{2,j} \\ \ldots \\ h_{j,j} \end{bmatrix} + h_{j+1,j} \ \underline{q}_{j+1}. \tag{15}$$

The following notations are introduced

$$Q_j = [\underline{q}_1, \underline{q}_2, \ldots, \underline{q}_j]. \tag{16}$$

and

$$H_j = \begin{bmatrix} h_{1,1} & h_{1,2} & \ldots & h_{1,j} \\ h_{2,1} & h_{2,2} & \ldots & h_{2,j} \\ 0 & h_{3,2} & \ldots & h_{3,j} \\ 0 & 0 & \ldots & \ldots \\ 0 & 0 & 0 & h_{j,j} \end{bmatrix}. \tag{17}$$

Combining the recurrence relationships (15) at all steps then yields the fundamental relationships of the Arnoldi algorithm

$$\Phi \ Q_j = Q_j \ H_j + h_{j+1,j} \ \underline{q}_{j+1} \ \underline{e}_j^T, \tag{18}$$

where $\underline{e}_j^T = \lfloor 0, 0, \ldots, 0, 1 \rfloor$. Furthermore

$$Q_j^T \ Q_j = I. \tag{19}$$

Consider now the eigenvalue problem

$$\Phi \ \underline{u} = \Lambda \ \underline{u}. \tag{20}$$

An approximate solution of this problem is sought within the Krylov subspace Q_j obtained after j step. The projection of $\underline{u}$ onto this subspace is

$$\underline{u} = Q \ \underline{s}, \tag{21}$$

where the subscript j was dropped for clarity. The eigenproblem (20) is now approximated as

$$Q^T \ \Phi \ Q \ \underline{s} = \hat{\Lambda} \ Q^T \ Q \ \underline{s}, \tag{22}$$

where $\hat{\Lambda}$ are the eigenvalues of this reduced eigenproblem. Using eqs. (18) and (19), together with the orthogonality of $\underline{q}_{j+1}$ to all previous $\underline{q}_j$ then yields

$$H\ \underline{s} = \hat{\Lambda}\ \underline{s}. \tag{23}$$

In summary, the eigenvalues of the upper Hessenberg matrix H approximate those of the original matrix Φ.

The Arnoldi algorithm is summarized here:

Algorithm 1
Choose an arbitrary starting vector $\underline{r}$*;*
$h_{1,0} = ||\underline{r}||$*;*
$\underline{q}_1 = \underline{r}/h_{1,0}$*;*
for $j = 1 : j_{MAX}$ *(Main Arnoldi loop)*
  $\underline{w} = \Phi\ \underline{q}_j$*;*
  $\underline{r} = \underline{w}$*;*
  for $i = 1 : j$
    $h_{i,j} = \underline{q}_i^T\ \underline{w}$*;*
    $\underline{r} = \underline{r} - h_{ij}\ \underline{q}_i$*;*
  end
  $h_{j+1,j} = ||\underline{r}||$*;*
  $\underline{q}_{j+1} = \underline{r}/h_{j+1,j}$*;*
end

At each step of the Arnoldi loop a new column of the upper Hessenberg matrix H is computed. Round-off errors greatly affect the performance of this algorithm. If a strict orthogonality of Q is not maintained, the algorithm fails to converge. Consequently, explicit re-orthogonalization of $\underline{q}_{j+1}$ with respect to all previously computed $\underline{q}_i$ using Gramm-Schmidt procedure is added at each step

$$\hat{\underline{q}}_{j+1} = \underline{q}_{j+1} - \sum_{i=1}^{j} (\underline{q}_i^T\ \underline{q}_{j+1})\ \underline{q}_i. \tag{24}$$

The QR algorithm [9] is then used to extract the eigenvalues $\hat{\Lambda}_i$ and eigenvectors $\underline{s}_i$ of H which are an increasingly accurate approximation to the eigensolution of Φ, *i.e.* $\Lambda_i \approx \hat{\Lambda}_i$ and $\underline{u}_i \approx Q\ \underline{s}_i$. The largest eigenvalues are the first to converge. The quality of this approximation can be readily evaluated

$$|\Lambda_i - \hat{\Lambda}_i| < ||\Phi Q\ \underline{s}_i - \hat{\Lambda}_i Q\ \underline{s}_i||, \tag{25}$$

Using eqs. (18) and (23) then yields

$$|\Lambda_i - \hat{\Lambda}_i| < |h_{j+1,j}||s_{i,j}|, \tag{26}$$

where $s_{i,j}$ is the last entry of the eigenvector $\underline{s}_j$. In N Arnoldi step, A is transformed into an $N \times N$ upper Hessenberg matrix H_N which eigenvalues are identical to those of A. However, the eigenvalues of H_j very rapidly converge to the dominant eigenvalues of A for $j << N$. The spacing between the dominant eigenvalues determines their rate of convergence .

The most important feature of the Arnoldi algorithm is that the matrix Φ whose eigenvalues are being computed is not explicitly manipulated. Considering algorithm 1, Φ only appears in the operation $\underline{w} = \Phi\ \underline{q}_j$. In other words, extracting the eigenvalues of Φ with the Arnoldi algorithm only requires the ability to perform the matrix multiplication $\underline{w} = \Phi\ \underline{q}_j$. This feature makes the Arnoldi algorithm ideally suited to the extraction of dominant eigenvalues of large, sparse matrices. Indeed, the sparsity of Φ can be used to compute $\underline{w} = \Phi\ \underline{q}_j$ in an efficient manner.

4 The Implicit Transition Matrix Approach

In section 2, a framework for assessing the stability of linear systems with constant or periodic coefficients was developed. The stability criterion is based on the spectral radius of the transition matrix. In the classical application of this approach, the transition matrix is explicitly evaluated first, then its eigenvalues are computed, as discussed in section 2.

The proposed *implicit transition matrix approach* is a method that extracts the dominant eigenvalues of the transition matrix *without the explicit computation of this matrix.* The method relies on the properties of the Arnoldi algorithm described in the previous section. As pointed out, this algorithm only requires the ability to perform the matrix multiplication $\underline{w} = \Phi\ \underline{q}_j$. For the problem at hand, this operation corresponds to the computation of the response $\underline{w}$ of the system after a period T to initial conditions $\underline{q}_j$. In other words, it is not necessary to explicitly compute the complete transition matrix Φ before extracting its eigenvalues. At each step of the Arnoldi algorithm, the operation $\underline{w} = \Phi\ \underline{q}_j$ is replaced by the evaluation of the response $\underline{w}$ of the system after a period T to initial conditions $\underline{q}_j$. Initial conditions are selected by Arnoldi algorithm from the subspace orthogonal to previously computed vectors.

If N steps are performed, all the eigenvalues of the transition matrix are computed exactly, and N integrations over a period T are required. In this case, the implicit transition matrix approach requires the same computational effort as the classical approach outlined in section 2, and yields identical results. However, the advantage of the implicit transition matrix approach is that an excellent approximation to the dominant eigenvalues of Φ can be obtained in $j << N$ steps, *i.e.* the stability of the system, which only depends on the spectral radius, can be assessed in $j << N$ steps. This results in considerable computational savings. It should be noted that the rate of convergence of the dominant eigenvalue depends on the spacing between these eigenvalues, not on the size of Φ. In other words, the convergence rate depends on the physical characteristics of the system (the spacing between the eigenvalues), but not on its size (the number of degrees of freedom used in the analysis). This makes the implicit transition matrix approach particularly well suited for stability analysis of systems involving a large number of degrees of freedom.

5 Numerical Applications

The numerical examples to be presented in this section deal with flexible, nonlinear multibody systems, *i.e.* a collection of bodies in arbitrary motion with respect to each other

while each body is undergoing large displacements and rotations with respect to a frame of reference attached to the body. The strain within each elastic body is assumed to remain small.

The elastic bodies are modeled using the finite element method. The use of beam elements will be demonstrated for multi-body systems. The location of each node is represented by its Cartesian coordinates in an inertial frame, and the rotation of the cross-section at each node is represented by a finite rotation tensor expressed in the same inertial frame. The kinematic constraints among the various bodies are enforced via the Lagrange multiplier technique. Although this approach does not involve the minimum set of coordinates, it allows a modular development of finite elements for the enforcement of the kinematic constraints.

The equations of motion resulting from the modeling of multi-body systems with the above methodology present distinguishing features: they are stiff, nonlinear, differential-algebraic equations. The stiffness of the system stems not only from the presence of high frequencies in the elastic members, but also from the infinite frequencies associated with the kinematic constraints. Indeed, no mass is associated with the Lagrange multipliers giving rise to algebraic equations coupled to the other equations of the system which are differential in nature.

Two novel time integration schemes for flexible, nonlinear multi-body systems have been developed [16, **?**, 8, 17]. The first is an energy preserving scheme that combines two features: an energy preservation statement for the elastic bodies and the vanishing of the work done by the forces of constraint. This results in exact preservation of the total energy for the nonlinear multi-body system and *unconditional stability* is achieved. The scheme exhibits second-order accuracy and has no numerical dissipation. The second scheme is an energy-decaying scheme that combines two features: an energy decay inequality for the elastic bodies and the vanishing of the work done by the forces of constraint. This results in the decay of the total energy of the multi-body system and *unconditional stability* is achieved. This scheme possesses third-order accuracy and high-frequency numerical dissipation. The tight control over the behavior of the total energy of the system afforded by these scheme is particularly important when studying the stability characteristics of dynamical systems. Indeed, if energy is created or dissipated by the numerical scheme used to integrate the equations of motion, the stability characteristics of the system will be modified. A physically unstable system could be stabilized by numerical dissipation, or vice versa, a physically stable system could be destabilized by energy created by the numerical process.

Examples of application of the proposed methodology to flexible multi-body systems are presented in this section and demonstrate its accuracy and computational efficiency.

5.1 Jeffcott Rotor with Isotropic and Anisotropic Bearings

The first numerical example deals with a flexible anisotropic shaft a with massive, circular rigid disk located at mid-span. This example will be used to validate the proposed methodology against analytical solutions. The shaft is connected to end flexible couplings, then to support bearing of finite stiffness, as shown in fig. 1. The elastic behavior of the bearings is represented by concentrated springs of stiffness k_y^b and k_z^b and viscous dampers of constants μ_y^b and μ_z^b. If $k_y^b \neq k_z^b$, the bearing is said to be anisotropic.

In order to validate the results of the implicit transition matrix approach, its predictions

will be compared with those obtained from a classical modal reduction technique applied to the physical system. The following modes were retained in the analysis: two transverse displacements and two rotations of the mid-span disk, and two transverse displacements, all measured in the inertial system. This corresponds to a total of eight degrees of freedom or sixteen states. If either shaft or bearings are isotropic, the equations of motions of this simple modal model can be cast as a set of equations with constant coefficients, and classical methods can be used to evaluate stability. However, when both shaft and bearings are anisotropic, the resulting system of equations will present periodic coefficients and Floquet theory must be used to obtain damping rates and frequencies of the system.

The proposed implicit transition matrix approach will be applied to a finite element discretization of the multi-body system without resorting to modal reduction techniques. The shaft, modeled by six shear deformable cubic beam elements, was connected to end flexible joints which in turns, are attached to the revolute joints. The relative rotation of one of the revolute joints was prescribed so as to obtain the desired shaft angular velocity Ω. Finally, the revolute joints are connected to the ground by means of flexible joints that model the elastic and viscous behavior of the bearings.

The anisotropic shaft of length $L = 1\ m$ has different bending stiffnesses in two orthogonal directions, $EI_y = 300\ N.m^2$ and $EI_z = 500\ N.m^2$, a mass per unit length $m_s = 3.39 \times 10^{-3}\ Kg/m$, and polar moment of inertia $I_{ps} = 3.4 \times 10^{-5}\ Kg.m$. The disk has total mass $M_d = 5\ Kg$, and polar moment of inertia $I_{pd} = 8.14 \times 10^{-2}\ Kg.m^2$. The physical properties of the elastic couplings, and isotropic and anisotropic bearings are given in Table 1. The complete model involves a total of 241 independent states. A time step size $\Delta t = 10^{-4}\ sec$ was used for integration in all cases.

At first, isotropic bearings are considered. In this case, the modal equations of motion can be written in the rotating system, resulting in differential equations with constant coefficient. The predictions of the simple modal approach have been compared those of the proposed approach. Since all finite element degrees of freedom are measured in the inertial system, the multi-body formulation results in equations with periodic coefficients. The implicit transition matrix approach was used to extract the three dominant eigenvalues of the system. The corresponding system frequencies and damping ratios were then extracted using eq. (10). Fig. 2 shows the classical, static instability zone (*i.e.* corresponding to a zero frequency) between the two lowest bending frequencies of the anisotropic shaft ($41.0 < \Omega < 46.8\ rad/sec$), and excellent agreement between the predictions of the two approaches is observed.

Next, the effect of damping is investigated. Damping in the rotating system will be modeled by viscous forces $\underline{F}_d^*$ proportional to the strain rates, $\underline{F}_d^* = \mu_s\ C^*\ \underline{\dot{e}}^*$, where μ_s is the damping coefficient, $\underline{e}^*$ the strains, and C^* the cross-sectional stiffness matrix. $\underline{F}_d^*$, $\underline{e}^*$, and C^* are all measured in a body attached coordinate system. On the other hand, damping in the non-rotating system will be modeled by viscous dampers of constant μ_b in the bearing supports. A shaft system with damping characteristics $\mu_b = 3\ N.sec/m$, and $\mu_s = 10^{-3}\ sec$ will be investigated using the modal formulation and the proposed implicit transition matrix approach. Fig. 3 shows the stability characteristics predicted by both approaches. At shaft speeds below the main instability zone, the two bending modes are damped, but this damping has little effect on the size of the instability zone ($41.0 < \Omega < 46.7\ rad/sec$). For higher shaft speeds, a small zone of stability is observed, and finally the system is again unstable for speeds $\Omega > 56.0\ rad/sec$. Note the axial frequency of the shaft denoted by a star shaped

symbol on the figures. This mode is not present in the modal solution, and although not damped, it does not lead to any instability, as expected.

Finally, the effect of bearing anisotropy is studied by using the stiffness characteristic listed in the third column of Table 1. The stability boundaries predicted by the two approaches in the absence of damping and with damping are presented in fig. 4 and 5, respectively. In the presence of anisotropic bearings, the single static instability zone observed in the previous cases breaks up into two static instability zones ($35.1 < \Omega < 36.7$ and $42.5 < \Omega < 45.4$ rad/sec)), separated by a dynamic instability zone (*i.e.* corresponding to a non zero frequency) ($38.8 < \Omega < 40.8$ rad/sec). When damping is added, the two bending modes present damping over the entire range of shaft angular velocity, in contrast with the isotropic bearing case, see fig. 3. Here again the instability zones are reduced by the addition of damping, but only very slightly.

The excellent correlation observed in all cases between the modal formulation and the implicit transition matrix approach clearly validates this latter approach. If the classical Floquet theory were used for the full finite element model, the evaluation of the transition matrix would require the computation of the response of the system for 241 independent initial conditions. In all cases presented here, the three dominant roots of the transition matrix converged with an accuracy $\varepsilon = 10^{-8}$ after eleven iterations only. In other words, the implicit transition matrix approach yields accurate stability information at $11/241 = 4.5\%$ of the computational cost of the classical Floquet approach. Table 2 presents convergence of four least-damped modes with respect to the number of iterations with error magnitudes predicted by algorithm.

Figs. 6 and 7 show the time history of the mid-span disk transverse displacements for anisotropic bearings, in the presence of damping, at rotor speeds $\Omega = 39.52$ and 43.21 rad/sec, respectively. These time traces confirm the results of the above stability analysis: at $\Omega = 39.52$ rad/sec the system is experiencing a dynamic instability, whereas at $\Omega = 43.21$ rad/sec a static instability is present. Note that these time traces only provide a qualitative assessment of stability. Indeed it is difficult to evaluate damping (or growth) rates from these traces. In contrast, the proposed method accurately predicts the damping (or growth) rates of the three least damped modes of the system. Furthermore, this more detailed information is obtained at a lower computational cost. The vertical lines appearing on the figs. 6 and 7 indicate the total integration time required to predict the three dominant eigenvalues of the transition matrix.

5.2 Slider Crank Mechanism under Periodic Load

The next numerical example deals with the slider crank mechanism shown in fig. 8. The angular velocity of the crank is prescribed as ω, and a periodic load $P(t) = P_0 + P_1 \cos(\omega t + \phi)$ is acting on the slider. The rigid crank has a length $L_c = 0.2$ m; the arm has a length $L_a = 2$ m, a bending stiffness $EI_a = 10$ $KN.m^2$, a structural damping $mu = 10^{-5}$ sec and a mass per unit length $m_a = 0.1$ Kg/m. The mass of the slider is $M = 0.1$ Kg. The various components of the model are connected by means of revolute joints. In the initial configuration, the crank is in the vertical position, *i.e.* $\theta_0 = \pi/2$.

If the arm is assumed to be rigid, the compressive force in the arm can be easily computed

as

$$F_a = P_0 + P_1 \cos(\omega t + \phi) + M L_c \omega^2 \left[\cos(\omega t + \theta_0) + \frac{L_c}{L_a} \cos(2\omega t + 2\theta_0) + \mathcal{O}\left(\frac{L_c}{L_a}\right)^2 \right]. \quad (27)$$

Neglecting the terms in $\mathcal{O}(L_c/L_a)^2$ and higher, as well as those in $\cos(2\omega t)$ and higher harmonics, this force becomes

$$F_a \approx Q_0 + Q_1 \cos(\omega t + \phi), \quad (28)$$

where

$$Q_0 = P_0 + \frac{L_c}{L_a} M L_c \omega^2 \cos(2\theta_0), \quad Q_1 = P_1 + M L_c \omega^2 \cos(\theta_0 - \phi). \quad (29)$$

Under these very restrictive assumptions, the arm can be viewed as a simply supported beam acted upon by the harmonic compressive force (28). This problem is known as the parametric excitation of a beam [1, 5], and Strutt diagram delineates the stable and unstable zones of the problem in terms of two non-dimensional parameters

$$\Omega = \frac{\omega}{2\omega_e \sqrt{1 - Q_0/P_e}}, \quad \zeta = \frac{1}{2} \frac{Q_1}{P_e - Q_0}, \quad (30)$$

where $\omega_e = (\pi/L_a)^2 (EI_a/m_a)^{1/2}$ is the lowest bending frequency of the arm and $P_e = \pi^2 EI_a/L_a^2 = 24.67\ KN$ the Euler buckling load for the simply supported arm.

It should be noted that the proposed implicit transfer matrix approach assumes that the governing equations of the system are linear equations with periodic coefficients. On the other hand, when modeled with a finite element based multi-body code, the present slider crank mechanism is inherently nonlinear since it involves finite rotations and nonlinear constraints. However, it is possible to study the stability of small perturbation about a periodic solution of the system. To this effect, a periodic solution of the problem was first obtained by integrating the system for two period with an artificially high value of structural damping $\mu = 10^{-3}$ *sec*. For the third period, the nominal damping value was used and the response of the system was considered to be the periodic solution. The stability of small perturbations about this periodic solution was then investigated with the help of the proposed implicit transition matrix approach.

The ratio of the periodic to the constant part of the applied load was $P_1/P_0 = 5$, and parametric studies were conducted for P_0 varying from 1 to 5 KN. The arm was modeled with three cubic beam elements for a total of 177 states. Fig. 9 shows the frequencies and damping rates of the five least damped modes of the system versus the constant part P_0 of the excitation force. The crank speed was $\omega = 201.06\ rad/sec$, and the phasing of the parametric excitation was such that $\Psi = \theta_0 - \phi = \pi$. Fig. 10 shows the corresponding results when $\Psi = 0$. The system becomes unstable when $P_0 = 4.25$ and 3.1 KN for $\Psi = \pi$ and 0, respectively. In order to validate these predictions, the analogy between the present problem and that of the parametric excitation of a beam was used. For the present choice of the parameters, $\Omega \in [0.133, 0.144]$ (see eq. (30)) when $P_0 \in [1, 5]\ KN$ and at the onset of instability, $\zeta = 0.50$ and 0.48, for $\Psi = \pi$ and 0, respectively. This compares favorably with

the stability boundary predicted by Strutt diagram, $\zeta = 0.53$. A closer agreement should not be expected given the assumptions involved in the analogy.

For the higher crank speeds, lateral vibrations of the arm become more significant, resulting in vibratory loads that are no longer negligible when compared to the externally applied loads. As a result, the nonlinear behavior of the system becomes more pronounced. Figs. 11 and 12 show the predictions obtained from a second set of simulations at $\omega = 64\ rad/sec$, and $\Psi = \pi$ and 0, respectively. The stability boundaries are found to be $P_0 = 4.75$ and 2.6 KN for $\Psi = \pi$ and 0, respectively. The corresponding non-dimensional parameters are $\Omega \in [0.261, 0.286]$ for $P_0 \in [1, 5]\ KN$ and at the onset of instability, $\zeta = 0.51$ and 0.38, for $\Psi = \pi$ and 0, respectively. Strutt diagram predictions for the corresponding case are $\zeta = 0.45$. As expected, the correlation is rather poor, since the assumptions required to derive the analogy are clearly violated in this case.

An alternative way of validating the results of the proposed approach is to simulate the response of the system using time integration. Fig. 13 shows the axial and transverse shearing forces in the flexible arm at the point where it connects to the slider for $\omega = 201.06\ rad/sec$, $\Psi = \pi$, and $P_0 = 4.25\ KN$, *i.e.* in the stable zone, whereas fig. 14 show the corresponding results when $P_0 = 4.50\ KN$, *i.e.* in the unstable zone. The responses depicted in these figures qualitatively confirm the switch from stable to unstable behavior at $P_0 = 4.25$ and 4.50 KN, respectively. In the stable regime, the axial force in the arm is nearly harmonic, and closely follows eq. (28). Furthermore, the amplitude of the transverse shearing force is small, about 16% of that of the axial force. This explains the relatively good correlation with the predictions of Strutt diagram. In the unstable regime, the transverse shearing force rapidly increases, and its magnitude becomes comparable to that of the axial force.

6 Conclusion

An implicit transition matrix approach for multi-body system stability evaluation was presented in this paper. This approach combines the results of classical transition matrix approach and of the Arnoldi algorithm for eigenvalue extraction. The explicit computation of the transition matrix is not required. One single integration of the multi-body system is needed at each step of the algorithm, resulting in considerable computational savings. This method is ideally suited for stability analysis of periodic systems involving a very large number of degrees of freedom.

Numerical examples have demonstrated the ability of the proposed implicit transition matrix approach to predict the regions of static and dynamic instability as well as the characteristic exponents of least-damped or unstable modes. Very fast convergence of the leading eigenvalues of transition matrix controlling the least-damped modes was observed. Because this convergence rate is independent of the number of degrees of freedom of the model, systems with a very large number of degrees of freedom can be treated efficiently. The proposed approach was shown to provide detailed stability information, whereas simulation of the system only provides a qualitative assessment of system behavior.

It should be noted that the implicit transition matrix approach can be viewed as a post-processing step. All that is required to use the method is the ability to predict the response of the system to a given set of initial conditions. Hence, it can be implemented using any

existing multi-body dynamic analysis code.

Acknowledgments

This research was sponsored by the National Rotorcraft Technology Center under contract NCC 2-945. Dr. Yung Yu is the contract monitor.

References

[1] V.V. Bolotin. *Nonconservative Problems of the Theory of Elastic Stability.* Pergamon Press Limited, Oxford, England, 1963.

[2] M.J. Goodwin. *Dynamics of Rotor-Bearing Systems.* Unwinm Hyman, London, 1989.

[3] M. Lalane and G. Ferraris. *Rotordynamics Prediction in Engineering.* John Wiley & Sons, New York, 1990.

[4] H. Hochstadt. *Differential Equations.* Dover Publications, Inc., New York, 1964.

[5] A.H. Nayfeh and D.T. Mook. *Nonlinear Oscillations.* John Wiley & Sons, New York, 1979.

[6] A. Cardona. *An Integrated Approach to Mechanism Analysis.* PhD thesis, Université de Liège, 1989.

[7] A. Cardona and M. Géradin. Time integration of the equations of motion in mechanism analysis. *Computers and Structures*, 33(3):801–820, 1989.

[8] O.A. Bauchau. Computational schemes for flexible, nonlinear multi-body systems. *Multibody System Dynamics*, 2:169–225, 1998.

[9] G.H. Golub and C.F. Van Loan. *Matrix Computations.* The Johns Hopkins University Press, Baltimore, second edition, 1989.

[10] G.H. Gaonkar and D.A. Peters. Review of Floquet theory in stability and response analysis of dynamic systems with periodic coefficients. In *R.L. Bisplinghoff Memorial Symposium Volume on Recent Trends in Aeroelasticity, Structures and Structural Dynamics, Feb 6-7, 1986*, pages 101–119. University Press of Florida, Gainesville, 1986.

[11] C.S. Hsu. Impulsive parametric excitation: Theory. *Journal of Applied Mechanics*, 39:551–558, 1972.

[12] C.S. Hsu. On approximating a general linear periodic system. *Journal of Mathematical Analysis and Applications*, 45:234–251, 1974.

[13] D.A. Peters and K.H. Hohenemser. Application of the Floquet transition matrix to problems of lifting rotor stability. *Journal of the American Helicopter Society*, 16:25–33, 1971.

[14] P.P. Friedmann, C.E. Hammond, and T.H. Woo. Efficient numerical treatment of periodic systems with application to stability problems. *International Journal for Numerical Methods in Engineering*, 11:1171–1136, 1977.

[15] W.E. Arnoldi. The principle of minimized iterations in the solution of the matrix eigenvalue problem. *Quarterly of Applied Mathematics*, 9:17–29, 1951.

[16] O.A. Bauchau and N.J. Theron. Energy decaying schemes for nonlinear elastic multi-body systems. *Computers and Structures*, 59:317–331, 1996.

[17] O.A. Bauchau and C.L. Bottasso. On the design of energy preserving and decaying schemes for flexible, nonlinear multi-body systems. *Computer Methods in Applied Mechanics and Engineering*, 169:61–79, 1999.

List of Tables

List of Figures

Property	Elastic couplings	Isotropic bearings	Anisotropic bearings
Linear stiffnesses [N/m]			
Axial	5.0×10^3	1.0×10^8	1.0×10^8
Transverse (y)	1.0×10^8	1.0×10^4	1.0×10^4
Transverse (z)	1.0×10^8	1.0×10^4	5.0×10^3
Angular stiffnesses [N.m/rad]			
Torsional	1.0×10^8	1.0×10^8	1.0×10^8
Bending (y)	10.0	1.0×10^8	1.0×10^8
Bending (z)	10.0	1.0×10^8	1.0×10^8

Table 1: Physical properties of the elastic couplings, and isotropic and anisotropic bearings.

Eigenvalue number	9 iterations	Eigenvalues after 10 iterations	11 iterations	12 iterations
1	-0.01 (0.18%)	0.0576 (0.02%)	0.0425 (0%)	0.0425 (0%)
2	-1.14 (0.18%)	-0.006 (0.31%)	0.0002 (0%)	0.0002 (0%)
3	-6.72 (1.79%)	-1.329 (0.10%)	-1.298 (0%)	-1.298 (0%)
4	-13.5 (1.35%)	-21.26 (1.05%)	-18.13 (0%)	-18.13 (0%)

Table 2: Damping of four dominant eigenvalues after 9, 10, 11, and 12 Arnoldi steps. The numbers in parenthesis indicate the predicted error on the corresponding eigenvalue.

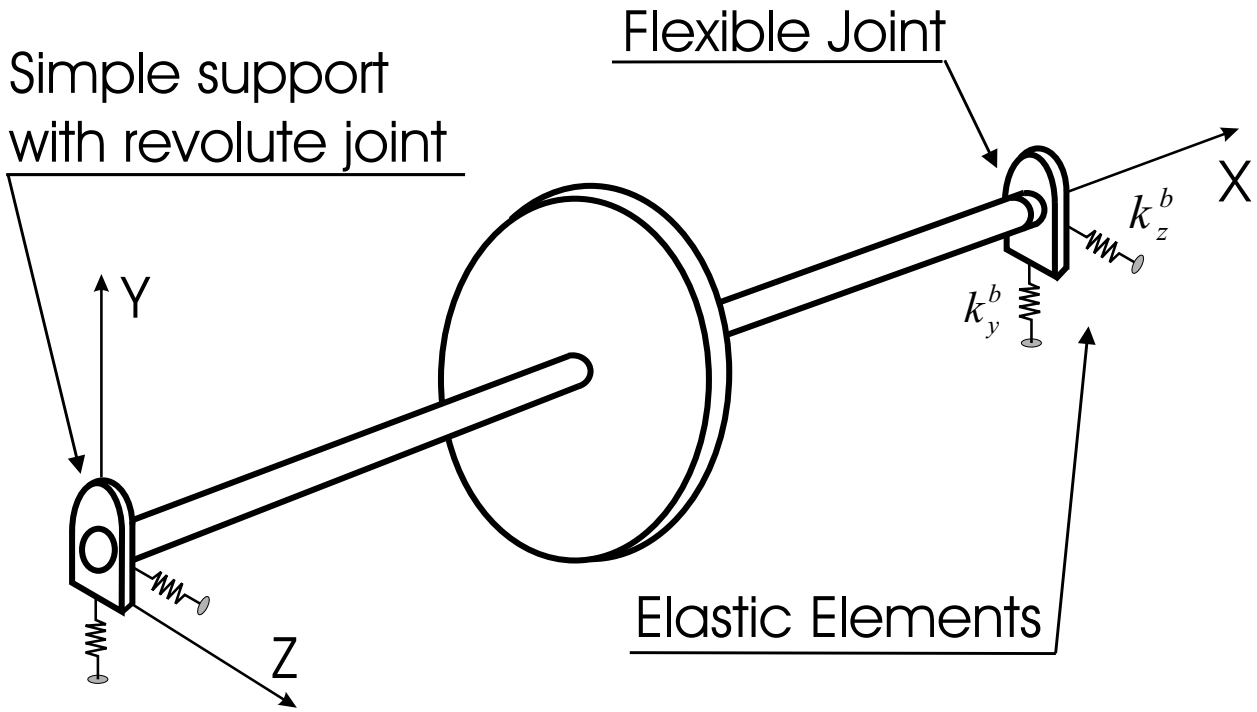

Figure 1: Jeffcott Rotor with flexible anisotropic bearings

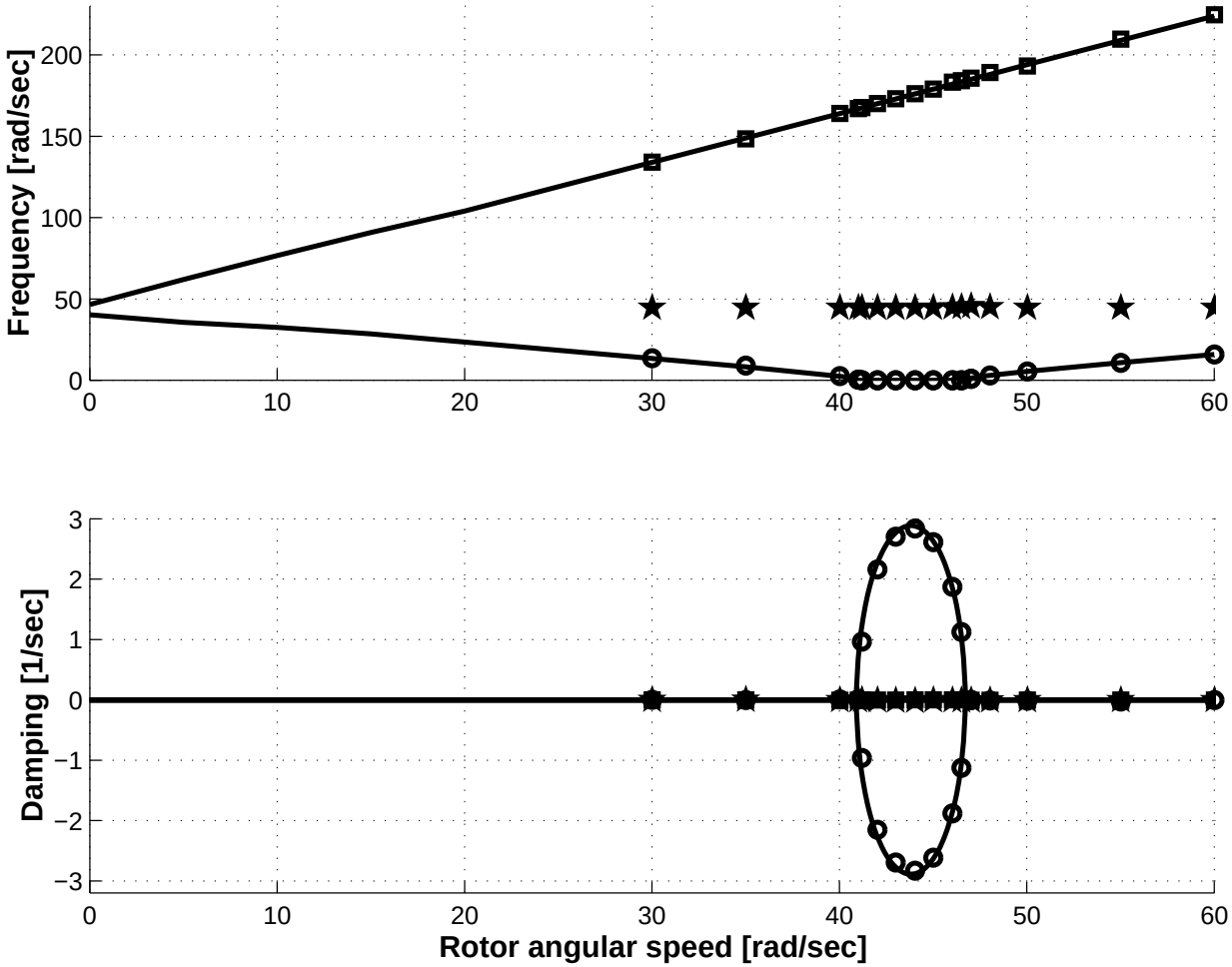

Figure 2: Frequencies and damping rates of the three least damped modes versus shaft angular velocity. Isotropic bearings, no damping. Solid line: modal solution; symbols: implicit transition matrix approach.

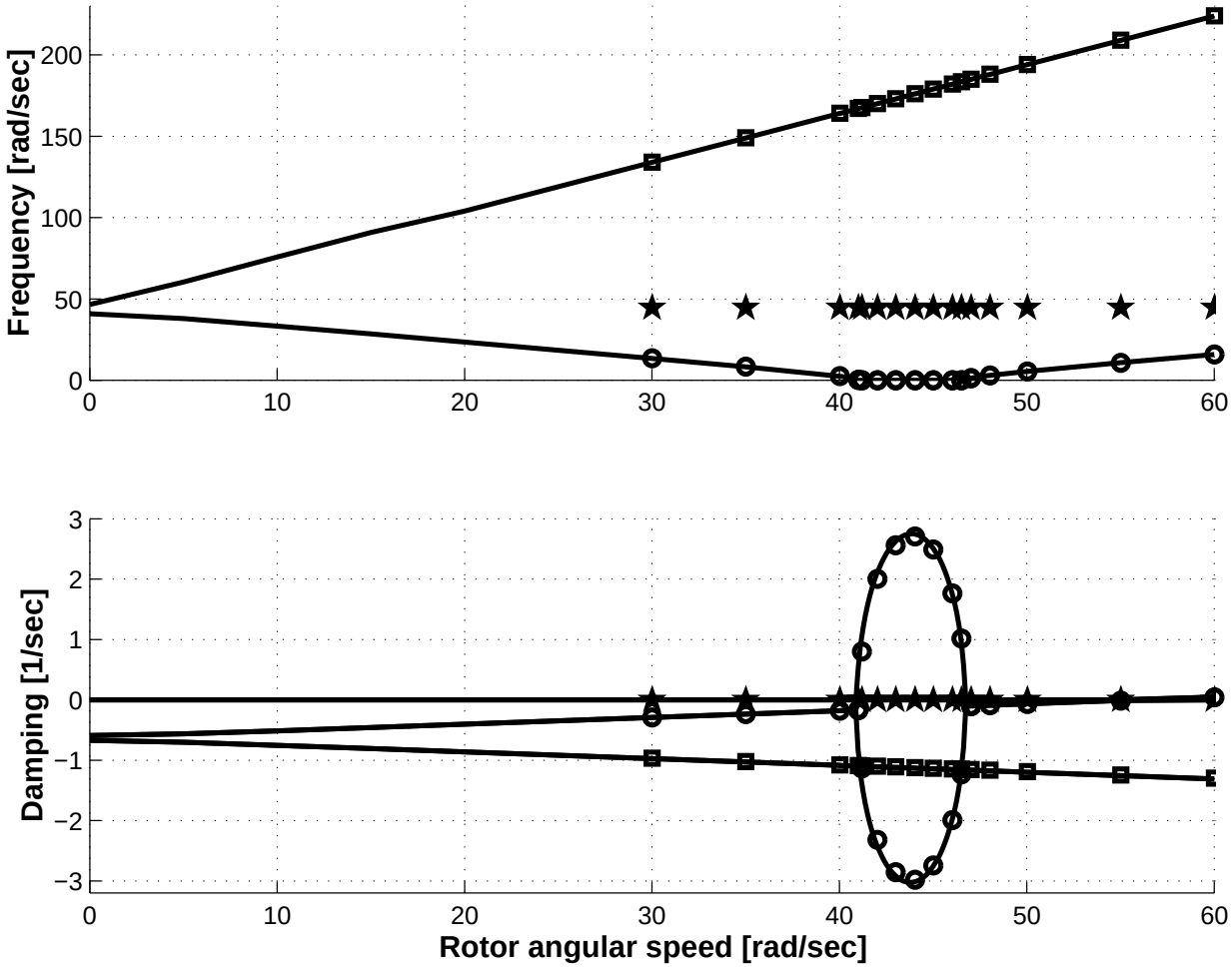

Figure 3: Frequencies and damping rates of the three least damped modes versus shaft angular velocity. Isotropic bearings. Solid line: modal solution; symbols: implicit transition matrix approach.

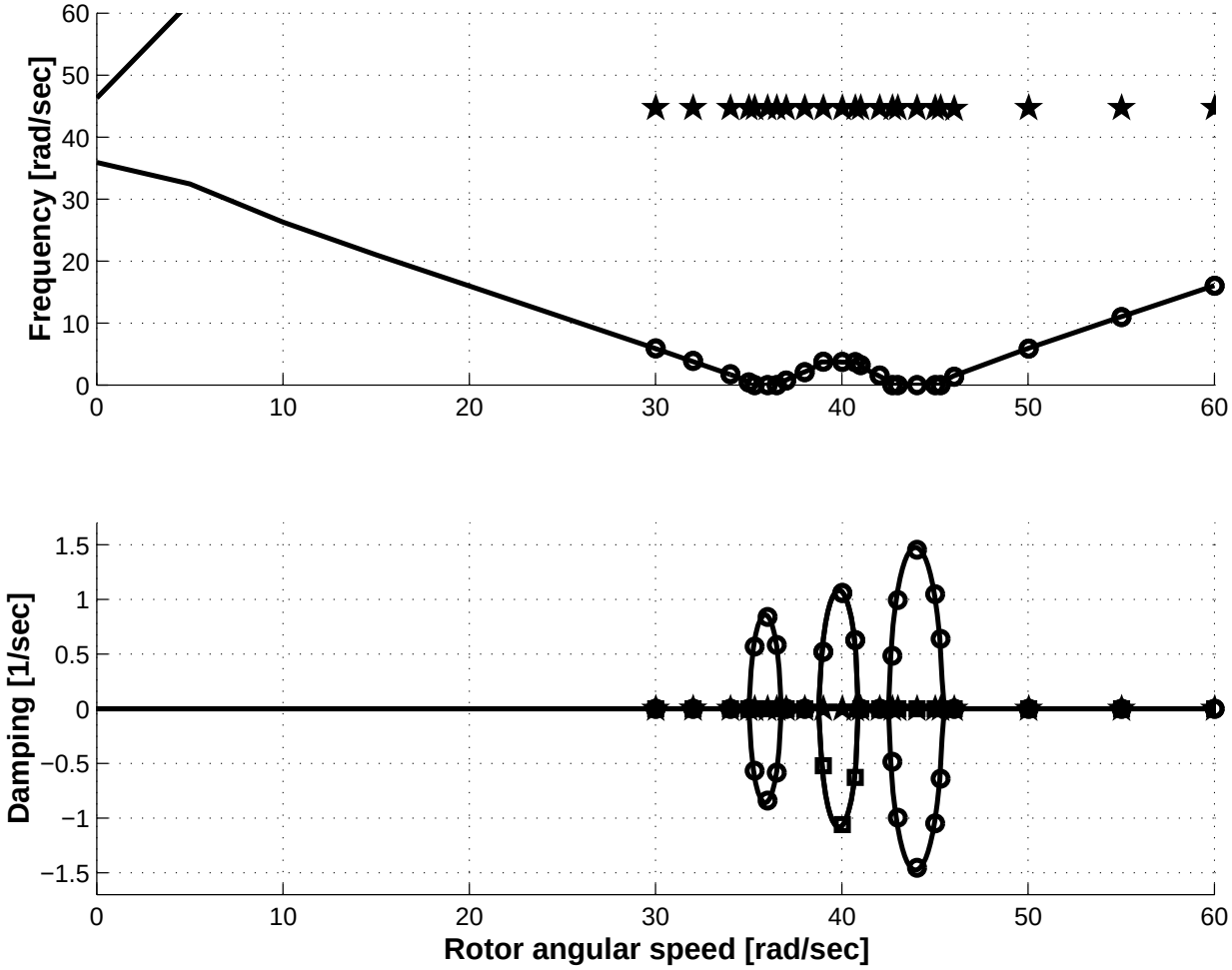

Figure 4: Frequencies and damping rates of least damped modes versus shaft angular velocity. Anisotropic bearings, no damping. Solid line: modal solution; symbols: implicit transition matrix approach.

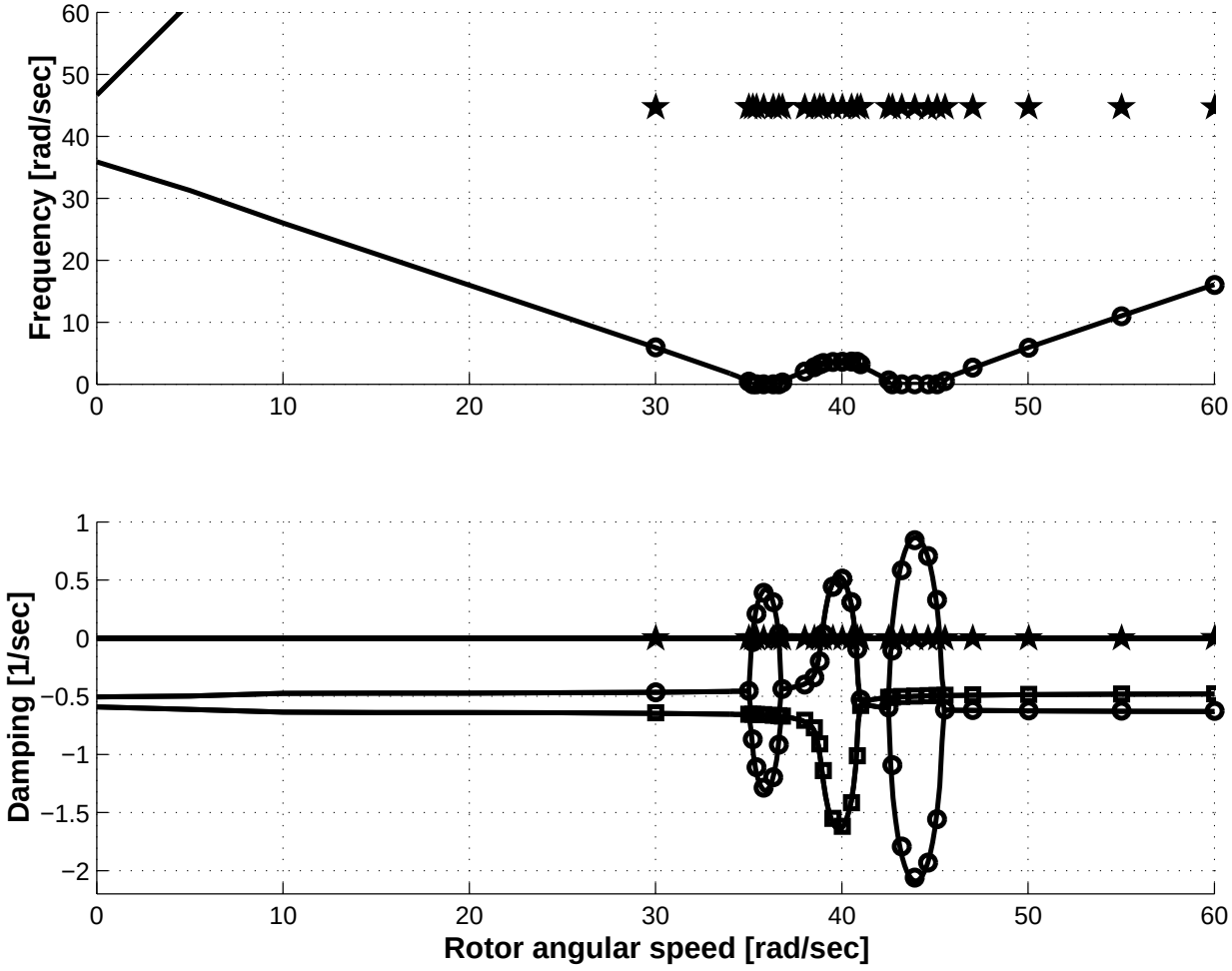

Figure 5: Frequencies and damping rates of least damped modes versus shaft angular velocity. Anisotropic bearings. Solid line: modal solution; symbols: implicit transition matrix approach.

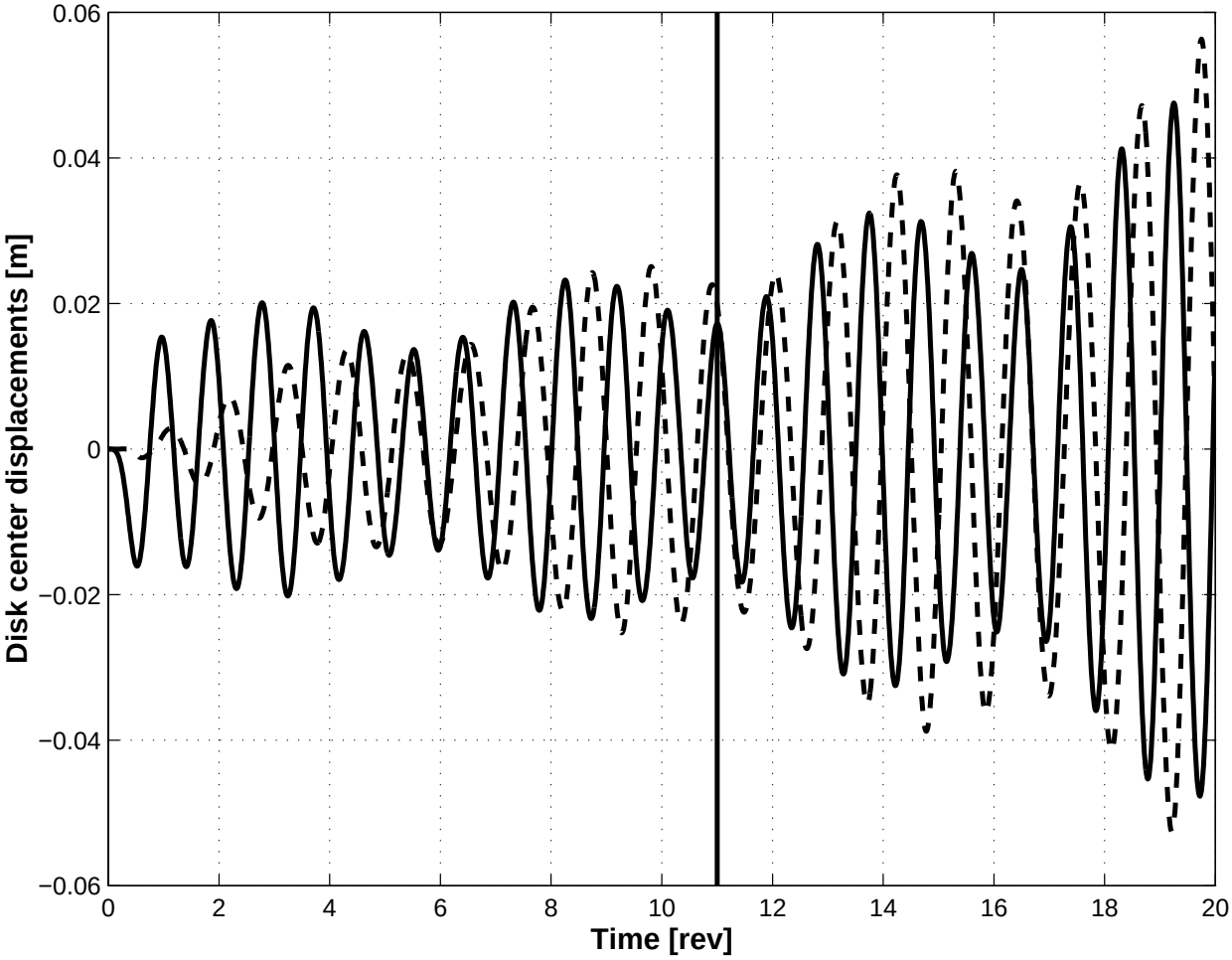

Figure 6: Time history of the mid-span disk transverse displacements u_y (solid line) and u_z (dashed line). Anisotropic bearings with damping. ($\Omega = 39.52\ rad/sec$)

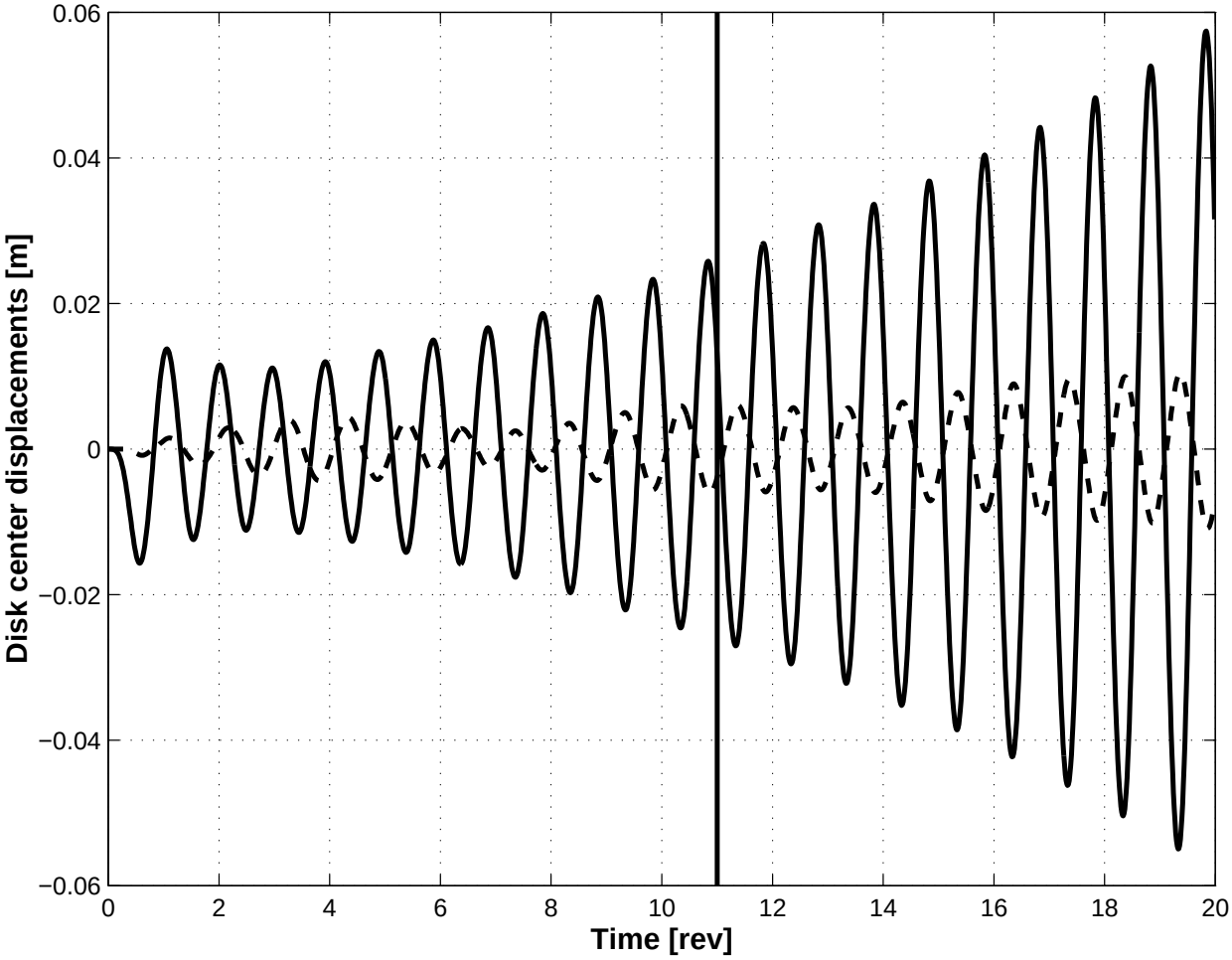

Figure 7: Time history of the mid-span disk transverse displacements u_y (solid line) and u_z (dashed line). Anisotropic bearings with damping. ($\Omega = 43.21\ rad/sec$)

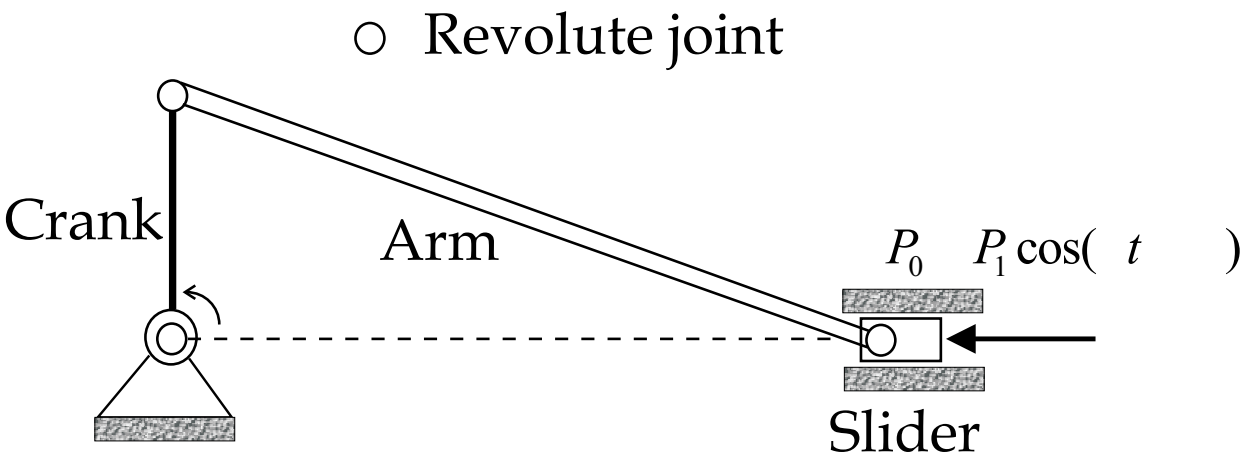

Figure 8: The slider crank mechanism in the reference configuration.

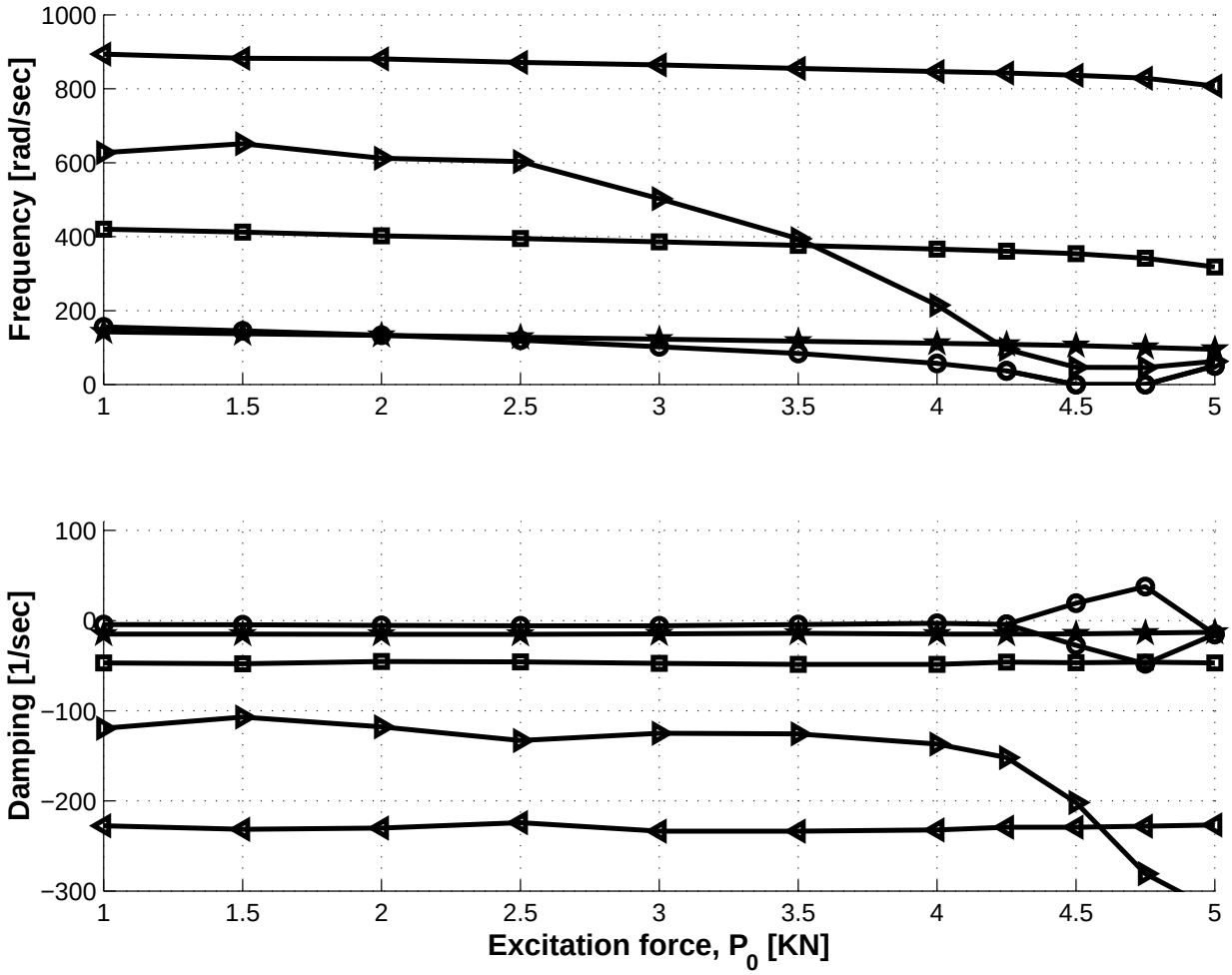

Figure 9: Frequencies and damping rates of the five least damped modes versus excitation force. $\omega = 201.06\ rad/sec$, $\Psi = \pi$.

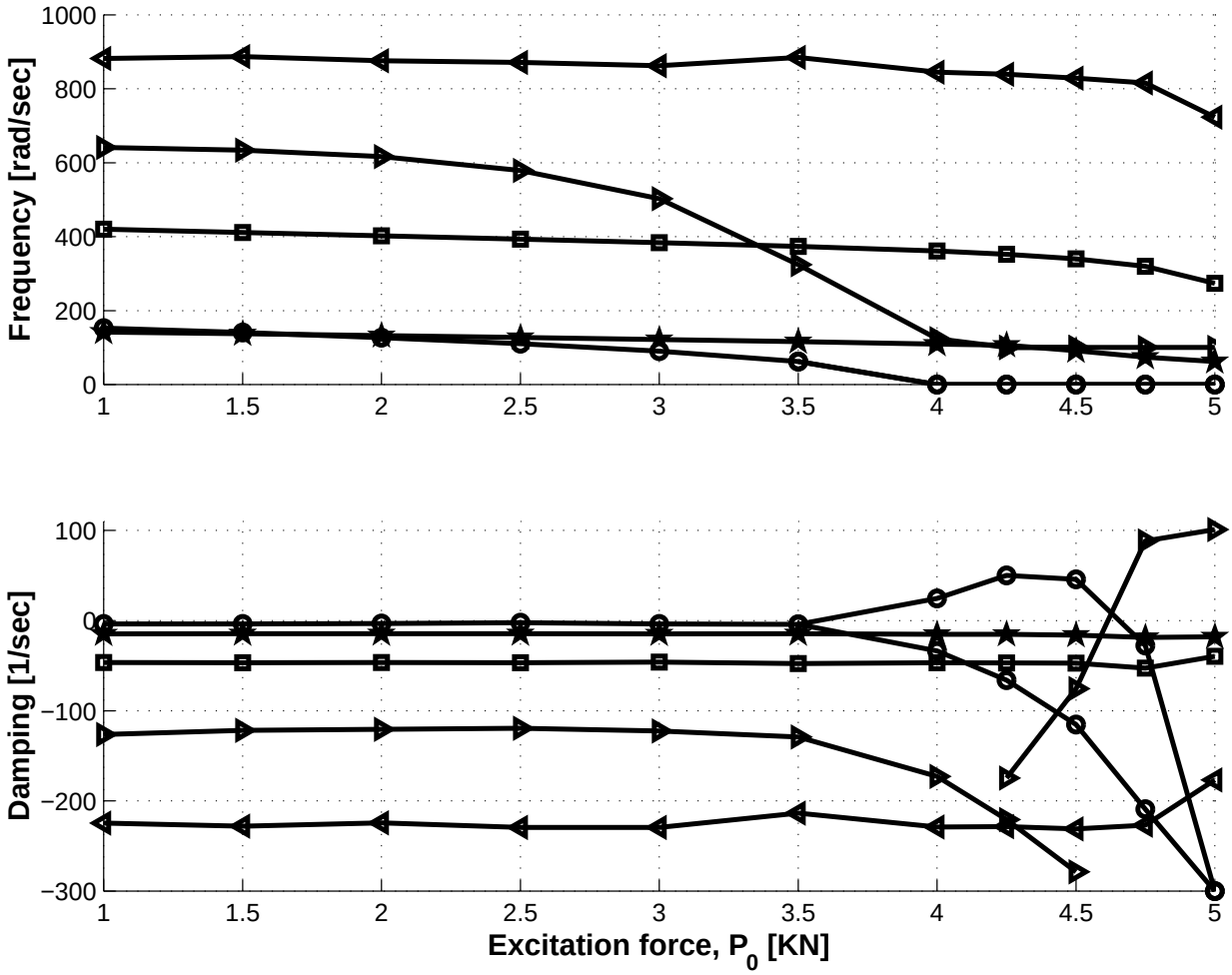

Figure 10: Frequencies and damping rates of the five least damped modes versus excitation force. $\omega = 201.06\ rad/sec$, $\Psi = 0$.

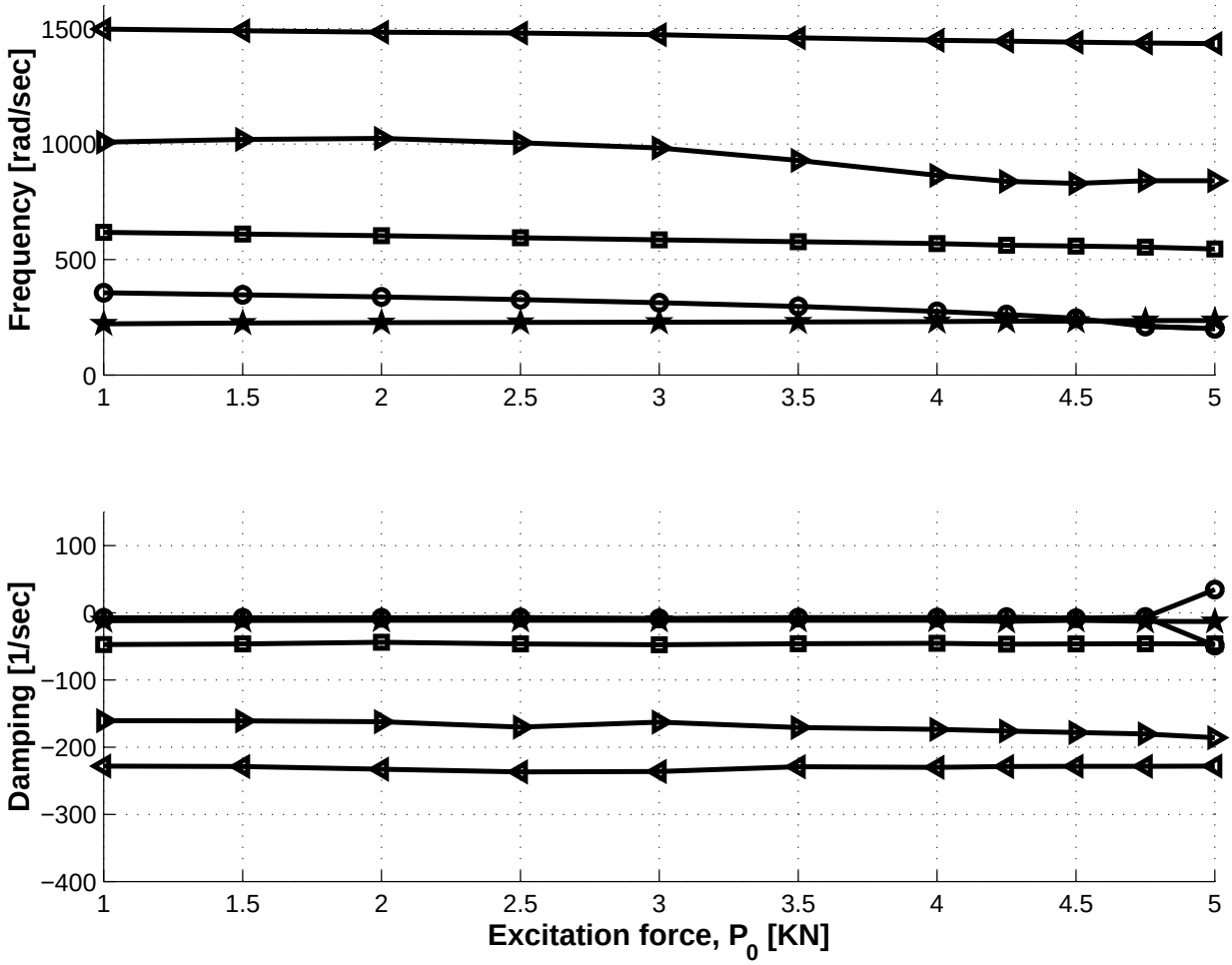

Figure 11: Frequencies and damping rates of the five least damped modes versus excitation force. $\omega = 402.12\ rad/sec$, $\Psi = \pi$.

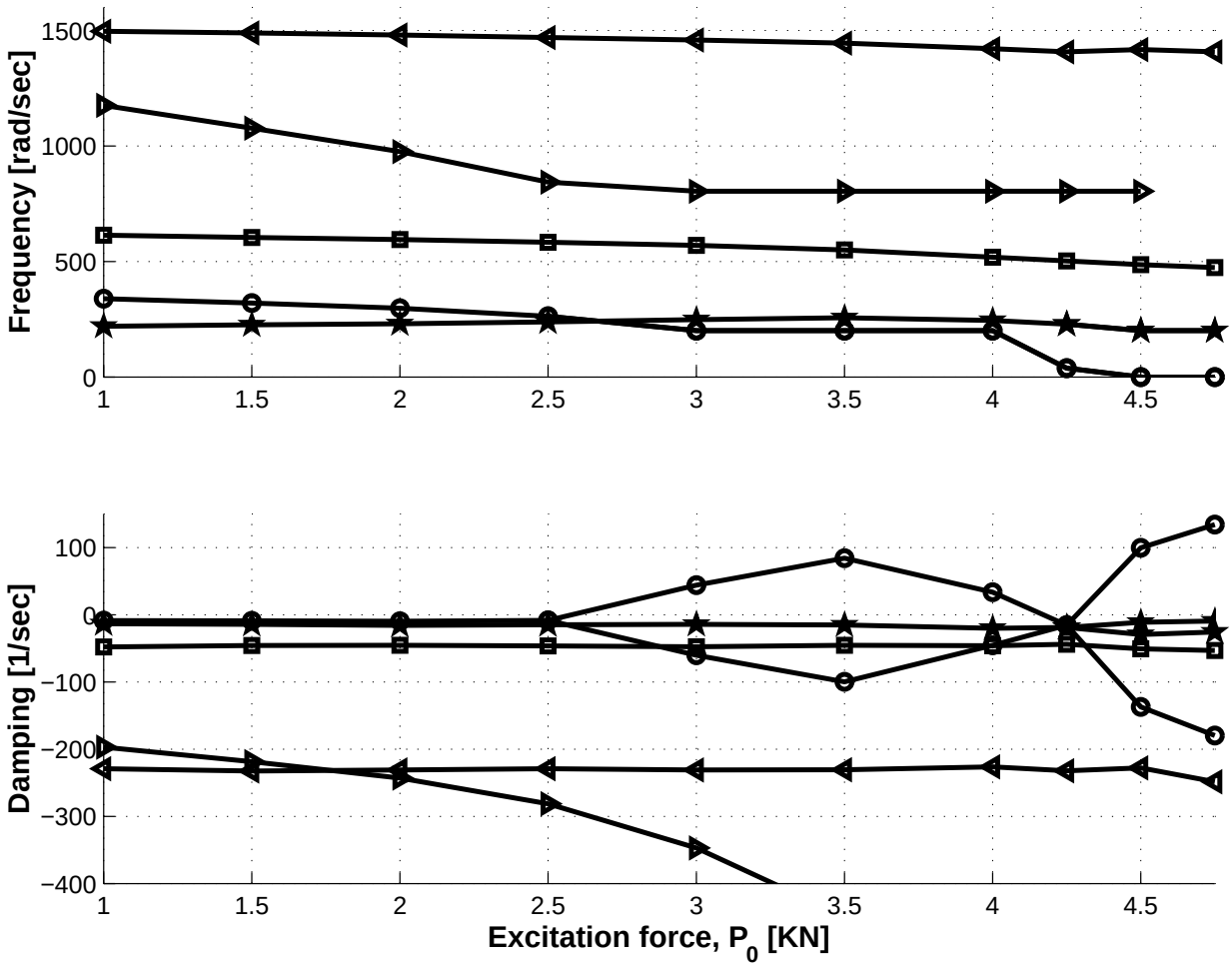

Figure 12: Frequencies and damping rates of the five least damped modes versus excitation force. $\omega = 402.12\ rad/sec$, $\Psi = 0$.

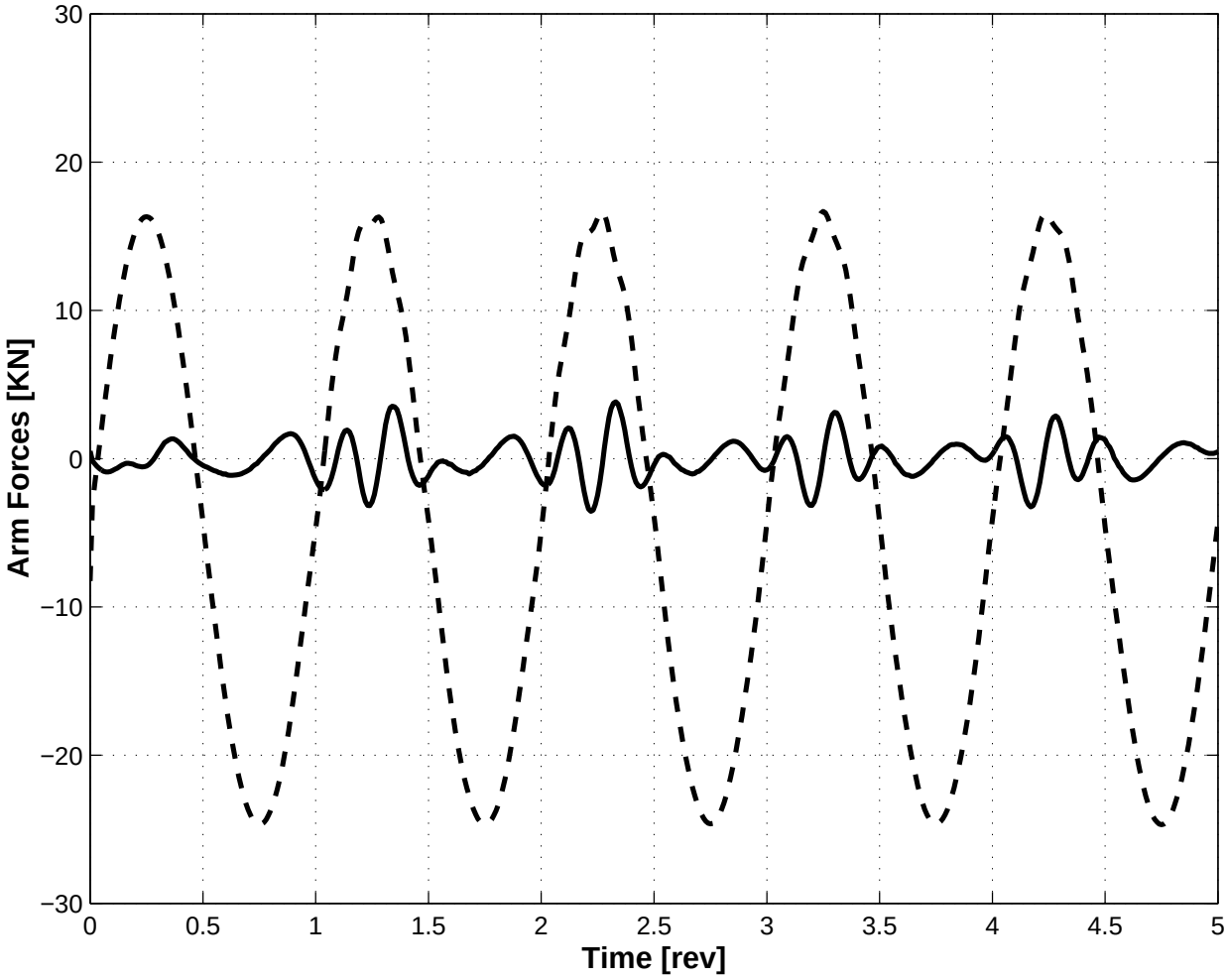

Figure 13: Forces at the arm slider connection point. Dashed line: axial force; solid line: transverse shear force. $\omega = 201.06\ rad/sec$, $\Psi = \pi$, $P_0 = 4.25\ KN$.

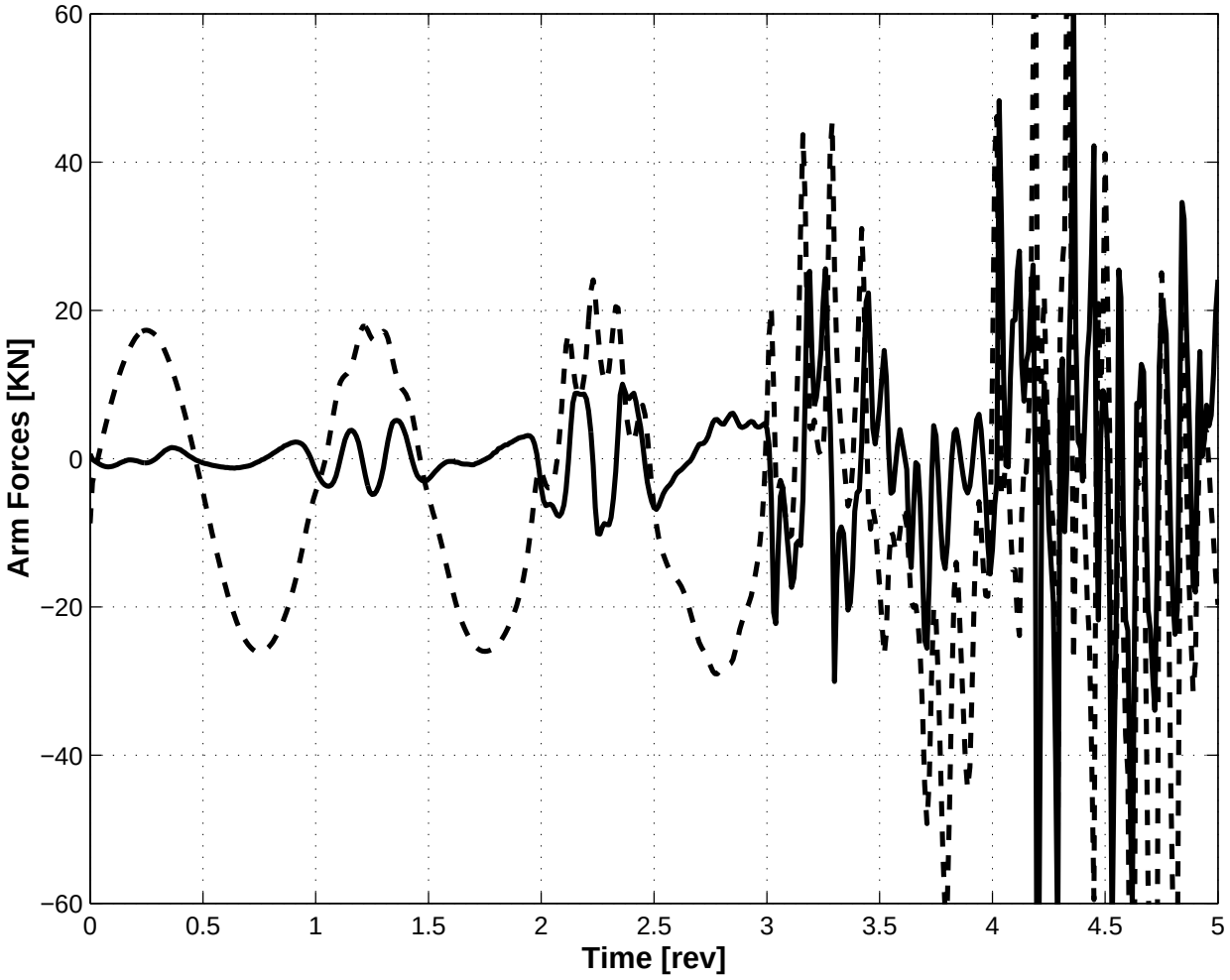

Figure 14: Forces at the arm slider connection point. Dashed line: axial force; solid line: transverse shear force. $\omega = 201.06\ rad/sec$, $\Psi = \pi$, $P_0 = 4.5\ KN$.